Materials Science in Semiconductor Processing 27 (2014) 433–445

Contents lists available at ScienceDirect

Materials Science in Semiconductor Processing

journal homepage: www.elsevier.com/locate/mssp

Towards a deeper understanding of physical and chemical properties of $Ag_2Hg\square I_4$ and $Cu_2Hg\square I_4$ defective crystals, from first principles calculations ☆

M. Dahmani [a], Tarik Ouahrani [a,b,*], M. Mebrouki [a,b], A.H. Reshak [c,d]

[a] Laboratoire de Physique Théorique, Université de Tlemcen, B.P. 230, 13000 Tlemcen, Algeria
[b] École Préparatoire Sciences et Techniques, département de Physique BP 165 R.P., 13000 Tlemcen, Algeria
[c] New Technologies - Research Center, University of West Bohemia, Univerzitni 8, 306 14 Pilsen, Czech Republic
[d] Center of Excellence Geopolymer and Green Technology, School of Material Engineering, University Malaysia Perlis, 01007 Kangar, Perlis, Malaysia

ARTICLE INFO

Keywords:
FP-LAPW
Phase transition
Second harmonic generation
Bonding properties

ABSTRACT

Pressure effect on the $Ag_2Hg\square I_4$ and $Cu_2Hg\square I_4$ defective compounds is studied from the point of view of the density functional theory. The pressure-induced changes chemical coordination and bonding nature were attributed to an order–disorder phase transition in the cation sublattice. Advantages of the analysis of the topology of the electron localization function (ELF) in the characterization of the chemical bonding change are illustrated. The ELF gives deep insight for interpreting the bonding behavior of the metallic defect rock salt structure while pressure is increasing. The calculated energy band gaps from mBJ(EV-GGA) potentials are used to predict electro-optic properties of the β phase of the $Ag_2Hg\square I_4$ and $Cu_2Hg\square I_4$ compounds. We make use of interband and intraband resonances contributions to analyze linear and nonlinear susceptibilities. The analysis makes semiconducting phase of the investigated compounds as promising for an intensive optoelectronic application.

1. Introduction

Attention towards comprehensive study of the behavior of defective materials exposed to variable thermodynamic conditions rests in many instances on detailed knowledge of the correlation between their observable properties and interactions around their constitutive atoms. The noteworthy structural and chemical features in the defective compounds present a paradigmatic case to investigate this correlation. In fact, defective crystal can be subject of interest for improving many properties, like formation energy and magnetic structure [1], electro-optical [2,3], and electrical conductivity applications [4]. Defective conductors in their α phases (like Ag_2HgI_4, Ag_2CdI_4, Cu_2HgI_4, Ag_2ZnI_4, Ag_3SnI_5 and Ag_4PbI_6) exhibit exceptionally high values of ionic conductivity within the solid state. Indeed, their conductivities often reach values of order of $1\ \Omega^{-1}\ cm^{-1}$, which are comparable to those observed in the molten state [5]. Thermo-ohmic transitions of the observed polymorphs of β-$Ag_2Hg\square I_4$ and β-$Cu_2Hg\square I_4$ ($\square$ denotes a cation vacancy) have been the subject of recent experimental [6] and theoretical investigations [5]. The vacancies in the silver structure are occupied by the copper ions in the copper structure and vice versa. Mcomber et al. [6] have undertaken Raman spectroscopy measures at some elevated temperatures to delineate the pressure–temperature phase diagram of the

☆ This Document is a collaborative effort.

* Corresponding author at: Laboratoire de Physique Théorique, Université de Tlemcen, B.P. 230, 13000 Tlemcen, Algeria.
Tel./fax: +213 43 20 18 24.
E-mail address: tarik_ouahrani@yahoo.fr (T. Ouahrani).

http://dx.doi.org/10.1016/j.mssp.2014.07.001
1369-8001/

investigated compounds. Above temperature equal to 70 °C at ambient pressure the two compounds transform from a β ordered electronic conductor into the α phase which displays mixed ionic and electronic conductivity and disorder of the Cu^+/Ag^+ and Hg^{2+} ions. There is a great recent interest in the applications of the β-$Ag_2Hg\square I_4$ and β-$Cu_2Hg\square I_4$ properties, making them good candidates as solid electrolytes [7]. Emphasis has been also placed on linear optical properties of these compounds (see Ref. [8]). However, the study was restricted to the first order of the dielectric function. Significant advances in the knowledge of linear and no-linear optical properties of β-$Ag_2Hg\square I_4$ and β-$Cu_2Hg\square I_4$ are possible, thanks to *ab-initio* studies that contribute and envisage possible applications in the industrial applications.

The analysis of solid–solid phase transitions involving dramatic changes in the localization pattern has become a major topic over the last years, thanks to some new available high pressure techniques. Despite the strong interest in the characterization of the properties of defective compounds, there are, to our knowledge, few experimental studies [9–12], of its properties at high pressures, probably due to the difficulties found in growing these crystals [13]. On the contrary, there are several measurements of the physical properties of other sulfide-based adamantine ordered-vacancy compounds ($ZnGa_2S_4$, $CdGa_2S_4$, $CdAl_2S_4$, and $HgAl_2S_4$) under pressure [14–18], and very recently in the Gallium based compounds like $CdGa_2Se_4$ [11], $HgGa_2Se_4$ [10] and $HgGa_2S_4$ [9,12].

Pressure constitutes a key parameter for precise tuning of interatomic distances, controlling the electronic structure and virtually all the interatomic interactions that determine materials properties. In order to determine the cause of higher values ionic conductivity of $Ag_2Hg\square I_4$ and $Cu_2Hg\square I_4$ compounds, Hull et al. [5], using temperature dependent powder neutron diffraction and impedance spectroscopy techniques, have found the following $\beta \rightarrow \alpha \rightarrow \gamma \rightarrow \varepsilon$ polymorphic sequence. Although the situation is complicated by the presence of the intervening γ hexagonal phase over a narrow temperature range, which interrupts the second-order transition, the ε phase is found rather as a *bcc* cubic structure.

Quantitative and rigorous formalisms based on the topological analysis of scalar fields as the electron density or the electron localization function (ELF) have been successfully used to study chemical changes induced by pressure in crystalline solids due to their ability to decompose the space in meaningful chemical fragments. Even the main applications of ELF to solid state studies have been centered on the description of intra-phase phenomena and the characterization of bonding [19,20]. Silvi and Gatti established numerous models to describe metallic systems [21]. Also, using the fact that topological procedure can decompose the crystal to a non-overlapping space. Recio et al. have devoted a number of works to follow up transition mechanism of pressure induced reconstructive [22] or displacive [23] transitions along many simple and complex compounds [23,22].

From a chemical point of view, a phase transition is characterized by a change in the number of bonds. Consequently, a measure of the pressure affecting bonds can be very informative. However, no much works have been devoted to track chemical bonding changes under pressure variation for this kind of entitled materials. Exploring the effect of pressure on chemical and physical properties of these materials can be guided by *ab initio* quantum mechanical calculations, avoiding expensive *trial and error* experimental processes. The electron localization function (ELF) [24,25] ability to unveil the nature of bonding led us to conduct a systematic study to investigate this change under the influence of pressure. Analyzing the optical properties of the entitled compounds will be also a part of this work.

The present paper is organized in three more sections. In Section 2, the computational details are briefly summarized. Section 3 is divided into three more sections, it contains the results of our analysis. The paper ends with the main conclusions of our work.

2. Method of calculation

The main outcome of our calculation strategy is to investigate optical response of the investigated compounds. The key piece in this study is to calculate momentum matrix elements and band structures. The highlighted clues of our investigation are the permitted interband and intraband transitions which obey to the selection rules [26]. In order to build our computational strategy, we have followed first-principles methodologies based on the density functional theory as implemented in WIEN2K [27] package. As a general guideline, structural and geometrical optimization tasks were calculated under the local density approximation (LDA) [28], and the generalized gradient approximation (GGA) using Perdew–Burke–Ernzerhof generalized gradient [29] parametrizations, whereas the modified Becke and Johnson (mBJ-LDA) potential [30] was used for electro-optic investigation. The latter improves the potential exchange by adding a semi-local orbital ($v_{x,\sigma}^{TB-mBJ}(\mathbf{r})$; there is no associated exchange functional E_x). The diagonalization of the Hamiltonian gives accurate eigenvalues, and thus the calculated band gaps of the materials come out in good agreement with experiments. For mBJ, the band gaps are considerably improved, while the effective masses are severely underestimated [31]. In the case of the EV potential, the equilibrium lattice constants are too large as compared to experiment and lead to an unsatisfactory total energy [32,33].

An extension of CRITIC [34] code has been recently developed to carry out a thorough topological analysis of the electron localization function (ELF) [24,25] in crystals. By means of this function we can calculate electronic charge transfer between atoms. This latter is intimately linked to the allowed electronic transitions between the valence and conduction band, and precisely to the linear response of the system to electromagnetic radiation described by means of the dielectric function $\varepsilon(\omega)$.

Another focus in our study is on analyzing the wave function. For this, we will use electron localization function tool (ELF). From a theoretical standpoint, ELF can be understood in terms of the excess of kinetic energy density introduced in the system by Pauli repulsion, $t_p(\vec{r})$. This quantity is computed by subtracting the bosonic

contribution $|\nabla\rho(\vec{r})|^2/8$ from the kinetic energy density of the system, $t(\vec{r})$. Re-scaling with respect to the homogeneous electrons gas like in the original definition provides the core of ELF, $\eta(\vec{r})$.

$$\eta(\vec{r}) = \frac{t_p(\vec{r})}{t_w(\vec{r})} = \frac{t(\vec{r}) - \frac{1}{8}\frac{|\nabla\rho(\vec{r})|^2}{\rho}}{c_F\rho^{5/3}(\vec{r})} \quad (1)$$

where c_F is the Fermi constant. According to this definition, the regions of electron pairing (where the Pauli principle is less relevant) would have a small η value. In order to inverse this relationship and map it in a closed interval, the final function was defined as follows:

$$ELF = \eta = \frac{1}{1+\eta^2(\vec{r})} \quad (2)$$

It can be easily seen that ELF runs from 0 to 1, and equals to 0.5 for the uniform electron gas. The final stone for the ELF analysis was led following Bader's idea of the topological analysis of the electron density [24,25]

3. Results and discussion

3.1. Structural properties

$A^{II}B_2^{III}X_4^{IV}$ family of ordered-vacancy compounds (OVCs) (semiconductors of the adamantine-type tetrahedrally coordinated) derive from the zinc blende or sphalerite ($F\bar{4}3m$) structure. They have a vacant cationic site in an ordered and stoichiometric fashion; i.e., a stoichiometric vacancy is located at a fixed Wyckoff position in the unit cell [35]. Our two compounds, Ag_2HgI_4 and Cu_2HgI_4, have doubled zinc blende unit cells along one of the *cubic* axes such that $c = 2a$. They are derived from chalcopyrite structure [36] by distributing the $4\times Cu/Ag^+$, $2\times Hg^{2+}$ and $2\times\square$ ($\square$ denotes a cation vacancy) in different ways over the eight cation sites. Their space groups are I $\bar{4}$ for the β-$Ag_2Hg\square I_4$ compound and I $\bar{4}$ 2m for the β-$Cu_2Hg\square I_4$ one. The Ag and Hg cations still form separate AgI_4 and HgI_4 tetrahedra, but the anion is now surrounded by one pair of Hg atoms, one Ag atom and one vacant site. The three cations surrounding the anion occupy nonequivalent crystal sites, so that the anion is free to move in all directions inside the $I(AgHg_2\square)$ tetrahedron. As a result, the equilibrium position of the anion is fixed by a set of independent coordinates (x, y, z). In the defect stannite β-$Cu_2Hg\square I_4$ structure, the Hg cations are distributed over equivalent crystal sites, so that a single Hg-I distance is present inside the $I(CuHg_{2\square})$ tetrahedron. This implies that the anion must be shifted by equal amounts along the **x** and **y** directions and its positional coordinates become (u, u, v).

We have completed extensive numerical analyses in order to secure stability of the computed zero pressure equilibrium values. We convert the calculated energy–volume (E,V) into static and finite-temperature pressure–volume (p,V) isotherms using numerical and analytical procedures coded in the GIBBS program [37]. Thermal contributions are included by means of a non-empirical quasi-harmonic Debye-like model. This approach only needs the set of (E,V) points and the calculated static bulk modulus to evaluate thermodynamic properties at different temperatures. At each volume, the internal parameters (x, y, z) or (u, u, v) are optimized to give the minimum total energy following a conjugate gradient algorithm. This procedure provides the dependence of the total energy on volume, which serves as an input for the determination of the equation of states (EOS). The athermal (static) computed lattice parameters for β-$Ag_2Hg\square I_4$ compounds are around 1.94% (LDA) smaller and 0.16% greater (GGA) than the observed data at room temperature [5]. For the β-$Cu_2Hg\square I_4$ compound shows values 4.24% (LDA) smaller and 1.04% greater (GGA) than the measured of ref [5] (see Table 1). For a range of pressure between 0 and 40 GPa, we note a displacement for the internal atomic position of $0.02\times a$ Å along the x/y direction and $0.01\times a$ Å along the z one, which means a large transformation of the structure along the z direction. The c/a ratio change approaches a $0.5\times c$ Å of the structure (a and c being the lattice parameters of the tetragonal structure).

Phase transitions studies for the highlighted compounds subject of this study are traditionally conducted under temperature effect [6]. However, many Raman scattering and optical absorption measurements [16,9–11] stipulate that the family of the defective crystals can also undergo order–disorder processes under the pressure effect. In this contribution, our calculations have been directed to compute the total energy and pressure-induced phase transition of the β phase of $Ag_2Hg\square I_4$ and $Cu_2Hg\square I_4$ in a wide range of lattice parameters ranging from 80 to 110% of the equilibrium geometries. The energy surface is then used to obtain the volume dependence of pressure at 0 K. These dependencies are gathered in Fig. 1(a) and (b). By means of the Gibbs energy differentiation ($\Delta G = 0$) (see Fig. 1(c) and (d)) between phases, we have found a pressure transition from I $\bar{4}$ to defect Rock salt phase equal to $P_t(LDA/GGA) = 4.4872/6.7544$ GPa for the $Ag_2Hg\square I_4$ compound, and from I $\bar{4}$ 2m to defect Rock salt phase equal to $P_t(LDA/GGA) = 18.4216/19.2427$ GPa for the $Cu_2Hg\square I_4$ one. The actual crystalline phases, exhibited in Fig. 1(a) and (b), show clearly that the I $\bar{4}$ and I $\bar{4}$ 2m structures for the β-$Ag_2Hg\square I_4$ and β-$Cu_2Hg\square I_4$ respectively lie in its local minimum energy, confirming the observed neutron diffraction data [5]. Raman measurements of Gomis et al. [10,11,9] confirm the existence of this defect rock salt structure at intermediate pressure. The $CdGa_2Se_4$ [11], $HgGa_2Se_4$ [10] and $HgGa_2S_4$ [9] naturally subject of temperature-dependent order–disorder transition also show pressure induced transformation at respectively, 23, 22 and 18 GPa. The authors found a change from tetrahedrally coordinated semiconductor phases towards octahedrally coordinated metallic phases, confirming their rock salt structure.

3.2. Electronic properties

Recently, Tran and Blaha proposed an orbital independent exchange semilocal potential (see Ref. [38]) by modifying the BJ exchange potential (see Ref. [39]) to reproduce the band energy gaps of solids as much as accurate in competition with that of the accurate but expensive local approximation plus

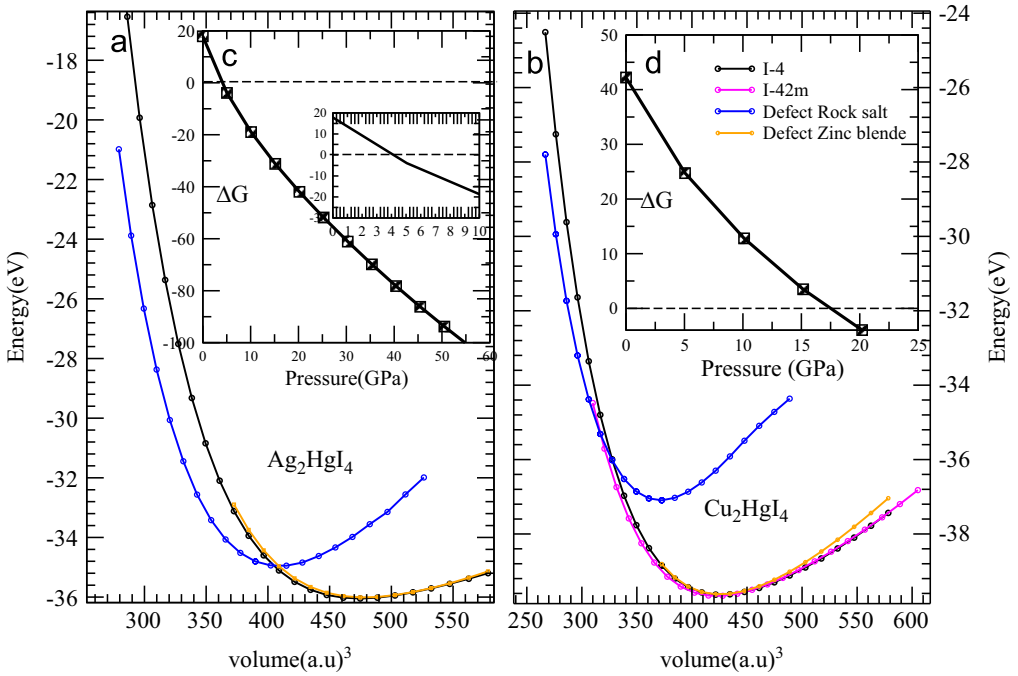

Fig. 1. (a) and (b) The plot calculated total energy versus volume and (c) and (d) calculated ΔG energies for all involved phase transitions of stannite $Cu_2Hg\square I_4$ and defect chalcopyrite $Ag_2Hg\square I_4$ compounds.

the dynamical mean-field theory (LDA+DMFT) [40] and the GW Quasi-particle [41] methods. The modified BJ exchange potential [38] can be reformulated as follows:

$$v_{x,\sigma}^{TB-mBJ}(\mathbf{r}) = \left(1.023\sqrt{\frac{1}{\Omega}\int_{\Omega}\frac{|\nabla\rho_\sigma(\mathbf{r}')|}{\rho_\sigma(\mathbf{r}')}d\mathbf{r}'} - 0.012\right) \times\left\{\frac{2\sqrt{[3]}\pi\rho_\sigma(\mathbf{r})e^{x_\sigma(\mathbf{r})/3}}{x_\sigma(\mathbf{r})}\left[\left(1+\frac{1}{2}x_\sigma(\mathbf{r})\right)e^{-x_\sigma(\mathbf{r})}-1\right] +\frac{3}{\pi}\sqrt{\frac{5}{12}}\left(\frac{\sum_{i=1}^{N_\sigma}\nabla\psi_{i,\sigma}^{*}.\nabla\psi_{i,\sigma}}{\sum_{i=1}^{N_\sigma}|\psi_{i,\sigma}|^2}\right)^{1/2}\right\} -\frac{2}{\pi}\sqrt{\frac{5}{12}}\left(\frac{\sum_{i=1}^{N_\sigma}\nabla\psi_{i,\sigma}^{*}.\nabla\psi_{i,\sigma}}{\sum_{i=1}^{N_\sigma}|\psi_{i,\sigma}|^2}\right)^{1/2}, \quad (3)$$

$$v_{x,\sigma}^{TB-mBJ}(\mathbf{r}) = c\times\left(v_{x,\sigma}^{BJ}(\mathbf{r})+\frac{1}{\pi}\sqrt{\frac{10t_\sigma(\mathbf{r})}{3\rho_\sigma(\mathbf{r})}}\right)-\frac{1}{\pi}\sqrt{\frac{10t_\sigma(\mathbf{r})}{3\rho_\sigma(\mathbf{r})}}, \quad (4)$$

where Ω is the unit cell volume, x_σ is related to the topology of the electron charge density, which can be obtained from the electron charge density, $\rho_\sigma(\mathbf{r})=\sum_{i=1}^{N_\sigma}|\psi_{i,\sigma}|^2$, $\nabla\rho_\sigma$ and $\nabla^2\rho_\sigma$ are gradient and Laplacian of the electron charge density, respectively, and $t_\sigma(\mathbf{r})=\frac{1}{2}\sum_{i=1}^{N_\sigma}\nabla\psi_{i,\sigma}^{*}.\nabla\psi_{i,\sigma}$, the electron kinetic-energy density. The mBJ exchange potential improves the potential exchange by adding a semi-local orbital. The diagonalization of the Hamiltonian gives accurate eigenvalues, and thus the calculated band gaps of the materials come out in good agreement with experiments.

Now we discuss our results pertaining to the electronic properties of the investigated compounds via the energy band structure and density of states. For the $Ag_2Hg\square I_4$ and $Cu_2Hg\square I_4$ in their β phase, the mBJ and Engel-Vosko (EV-GGA) [42] calculations predict that both valence band maximum (VBM) and conduction band minimum (CBM) are located at Γ point resulting in a direct band gap ($\Gamma_c-\Gamma_v$). The calculated energy band gaps from mBJ(EV-GGA) potentials are found equal to E_g=1.9(1.65) eV and E_g=1.50(1.42) eV for the $Ag_2Hg\square I_4$ and $Cu_2Hg\square I_4$ compounds respectively, (see Fig. 2). For the sake of comparison, we have found only two rare experimental reports which give respectively a measure of the band gap of 1.9/1.96 eV and 2.1 eV at room temperature for the β-$Cu_2Hg\square I_4$ and β-$Ag_2Hg\square I_4$ compounds [5,43].

Let us turn to density of state (DOS) and its partial decompositions, which are indeed outstanding. Partials DOS for the β and Rock salt phases of the studied materials are gathered in Fig. 3. For the semiconducting β phase of our compounds, we can see in Fig. 3 that: the low-energy set of the valence bands ranging from −14 to −13 eV arises mainly from the I 5*s* states. We notice that there is a strong hybridization between Ag/Cu–p and I *d* orbitals localized around the range of −6 eV to Fermi level. The intermediate energy subbands situated at about −8 eV and −6 eV consist entirely of Hg *d* and Hg *s* states, respectively. The top of the valence band (VB) and the bottom of the conduction band (CB) are mainly composed of I 5*p*/I-d binding levels and Hg 5*s* antibinding levels, respectively. A careful analysis of this Fig. 3 shows that while going to the Rock salt metallic phase the *s*-, *p*-, and *d*-orbital contributions shift to the Fermi level.

3.3. Bonding properties

A consistent and physically sound study of the chemical bonding under external pressure effect requires an adequate method [22]. For this, we have chosen accordingly to use

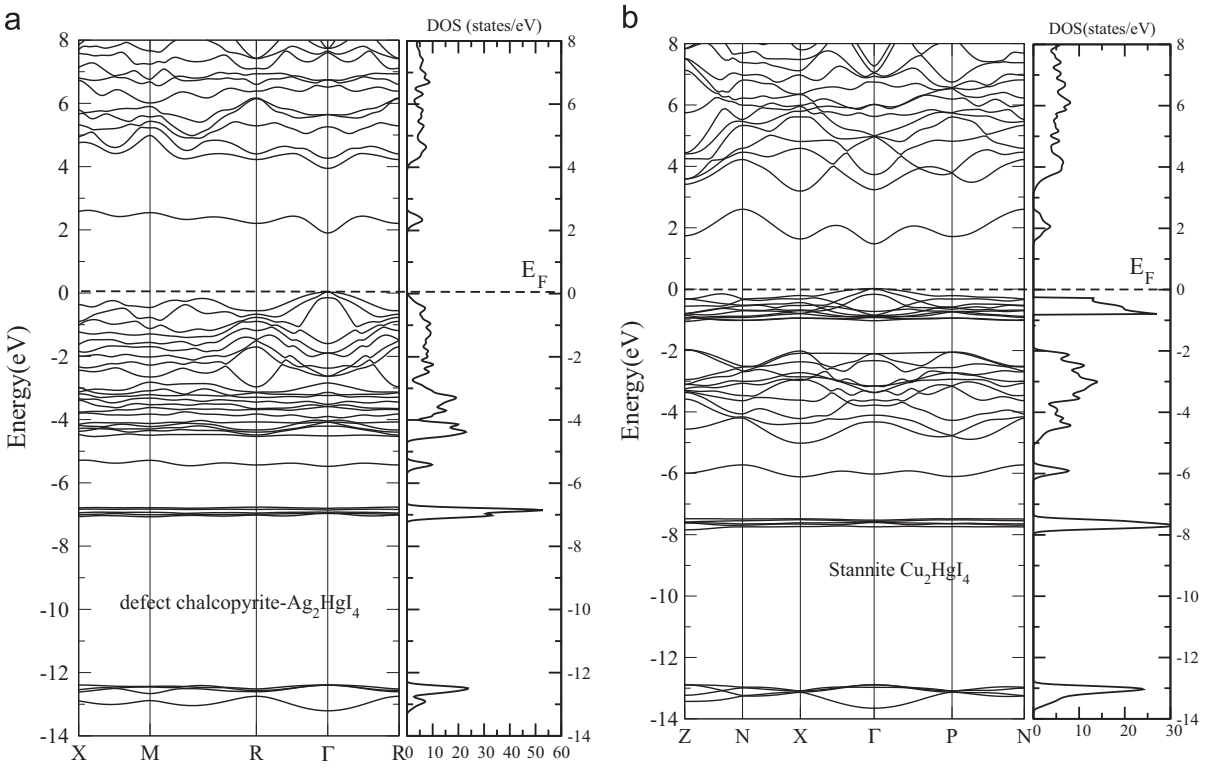

Fig. 2. Mbj-LDA band structure plot along the height symmetry points of stannite $Cu_2Hg\square I_4$ and defect chalcopyrite $Ag_2Hg\square I_4$ compounds.

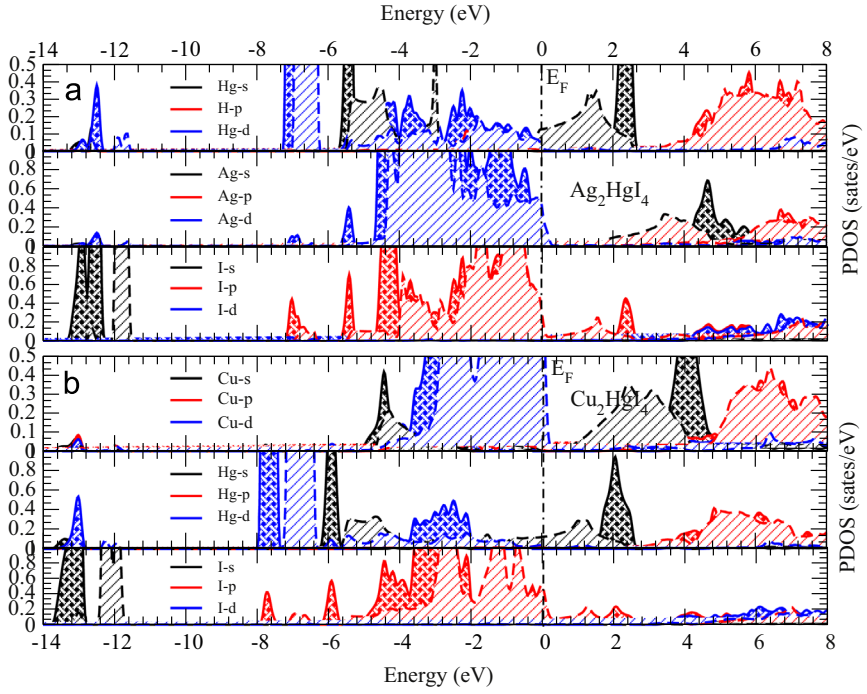

Fig. 3. Calculated partials density of states within the mBJ-LDA of the investigated compounds, crossed lines for β phase and angled lines for defect rock salt phase.

Electron localization function (ELF) formalism [24,25]. This method has shown its evidence in several studies as an excellent alternative to a simple representation of the charge density. As pointed out by Contreras-García et al. [44], the ELF exhibits maxima at the most probable positions of localized electron pairs and each maximum is surrounded by a basin in

which there is an increased probability of finding an electron pair. These basins correspond to the qualitative electron pair domains of the Valence Shell Electron Pair Repulsion (VSEPR). Besides, this kind of exhaustive partition has, in the solid state, the advantage of enabling an unequivocal assignation of basin contributions to many properties of the solid [22]. ELF

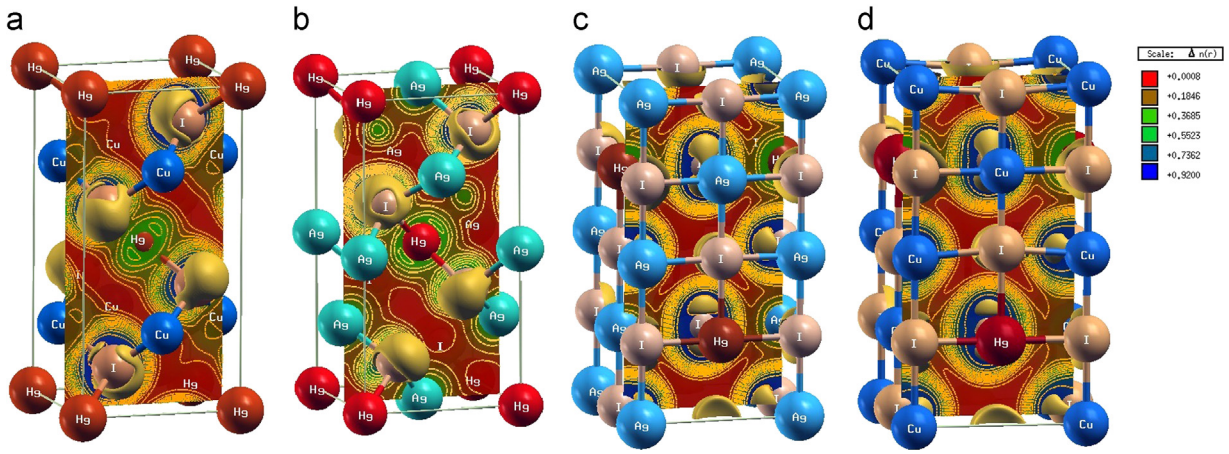

Fig. 4. 2D contour plot of the electron localization function for ELF=0.83 for : (a) stannite $Cu_2Hg\square I_4$, (b) defect chalcopyrite $Ag_2Hg\square I_4$, (c) defect rock salt $Ag_2Hg\square I_4$ and (d) defect rock salt $Cu_2Hg\square I_4$.

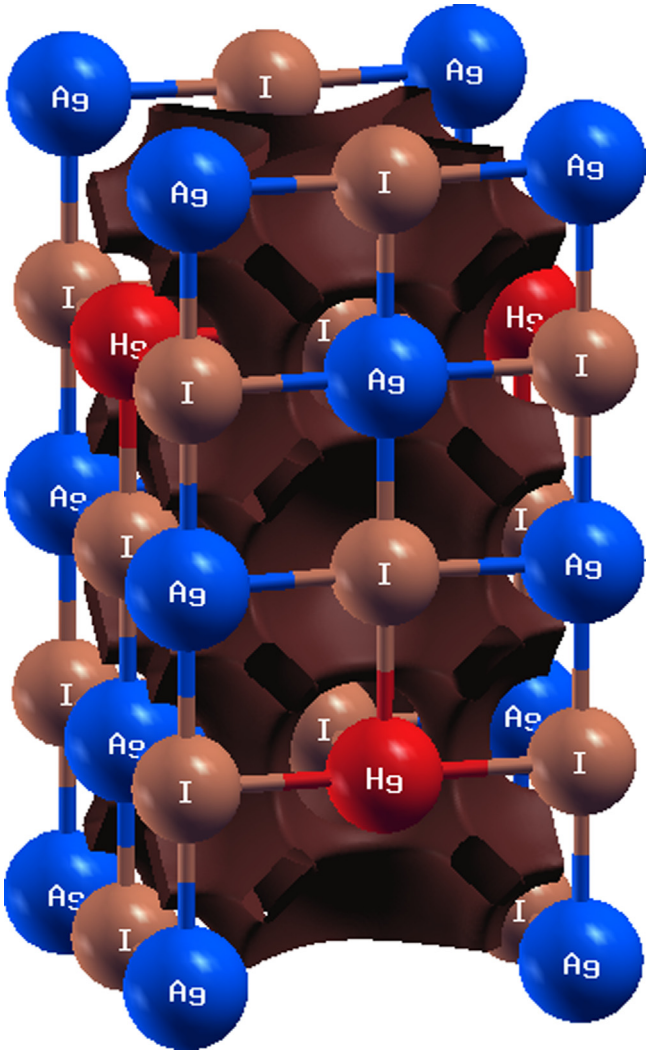

Fig. 5. Localization domains of the channels in metallic defect rock salt $Cu_2Hg\square I_4$, $ELF = \eta = 0.36$.

gradient encloses 3D regions or basins that can be bed-fellowed with electron shells, bonds, or lone pairs. These basins can be partitioned in finite, disjoint, and space filling regions as in the case of the atom in molecule approach [45]. Each of these basins contains a maximum or attractor of ELF, and between two of these attractors we can find a first-order saddle point whose ELF value provides details about the interaction between the corresponding basins. Fig. 4 displays ELF iso-surface plots of the $Ag_2Hg\square I_4$ and $Cu_2Hg\square I_4$ compounds in its semiconducting β and metallic Rock salt phases. Regarding the β phase of our structures, the ELF values of the Iodine sites are approximatively equal to one; showing the strong localization of the circulars attractors, while those of the Hg, Cu/Ag sites have a rather low ELF value approaching $\eta=0.36$. The non-spherical contours of the Iodine anion infer that covalent bonds exist in this system. Bader charge analysis proves this judgement as we calculate the degree of covalency [46]. Thus, the situation of the β phase on a topological van Arkel–Ketelaar diagram would correspond to the covalent ionic edge, much closer to the covalent than to the ionic vertex. The situation of defect Rock salt phase is a little different. As a signature of metallic behavior, the ELF attractors

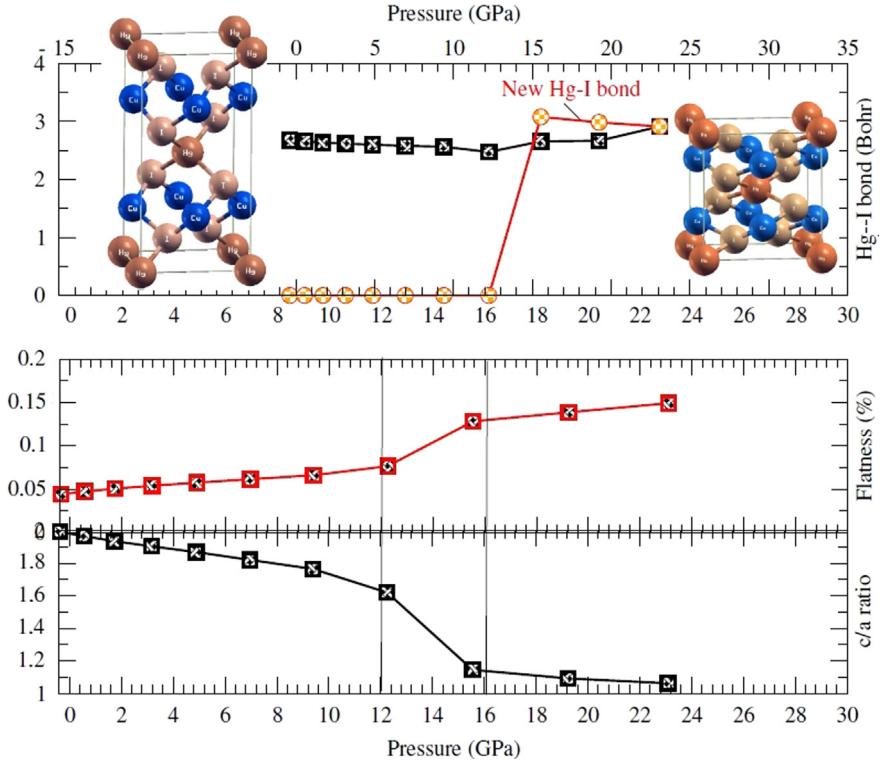

Fig. 6. Top, Hg–I bonds as a function of pressure and bottom, flatness (fa) and (c/a) ratio versus pressure of the β-$Cu_2Hg\square I_4$ compound.

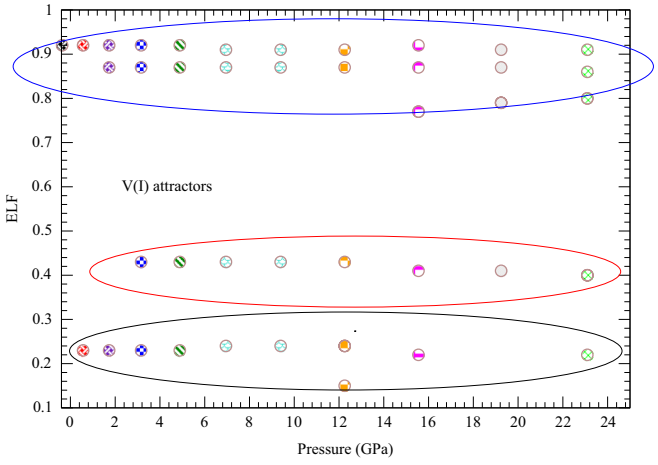

Fig. 7. Evolution versus pressure of valence attractors of three V(I) basins for the β-$Cu_2Hg\square I_4$ compound.

form a connected network. The charge density is relatively flat, which facilitates the electronic conduction.

From the structures of the right side of Fig. 4, it is clearly shown that the ELF maps of metallic systems present large areas within which the electron localization is nearly constant and close to the value $\eta=0.5$. These regions are connected one to the other by channels which form infinite one-, two-, and three-dimensional networks according to the conductivity directionality [47], see Fig. 5.

The phase transition from semiconducting to metallic structure engenders some interesting remarks: the main source of the phase reorganization under pressure is the achievement of a more efficient atomic packing by means of coordination changes. As pressure increasing on the β structure of our compounds, a shortening of nearest neighbor distances occurs. This shortening is accompanied by a raise in the chemical potential (μ) of the solid. Because the chemical potential always increases with pressure (at constant temperature), volume is reduced while keeping μ as low as possible. The procedure continues up to a stage where the increase in connectivity becomes energetically competitive with the shortening of distances, and eventually a phase transformation to a more denser coordination occurs. Analysis of Fig. 6 stipulates that while increasing pressure the flatness grows drastically beyond the transition pressure values. After this threshold P_t a new coordination are created (see the top of Fig. 6). The emergence of coordination from Hg four-fold to Hg five-fold coordinated can be characterized by two sets of movements: the atomic displacement and the unit cell strain, which are mainly a reduction of the c/a ratio. Fig. 6 helps to better understand the behavior of the c/a ratio under compression (In fact, c/a ratio is considered as a measure of cation-vacancy disorder, which means that cation disorder is increasing with pressure). This picture can be visualized in Fig. 7: there is an increase in the number of basins for the ELF attractors $V(I)$. This change is related to the changes in the atomic environment and the energetic profile. We have observed that the I–I and the Hg–I bonds number increases just after the transition state is reached, for the vacancy □ are evidently the more compressible. This gives a rapid decrease of the □–I distance leading to a new atomic order (defect Rock salt phase).

3.4. Optical properties

Another issue that must be addressed regards the optical properties of the entitled compounds. Some information may be gained by examining the linear response and the second harmonic generation properties. The second harmonic generation (SHG) process involves the absorption of two equal photons and the emission of a third one with twice their energy due to energy conservation. In order to conduct an adequate study on optical properties, it is essential to start with the calculation of

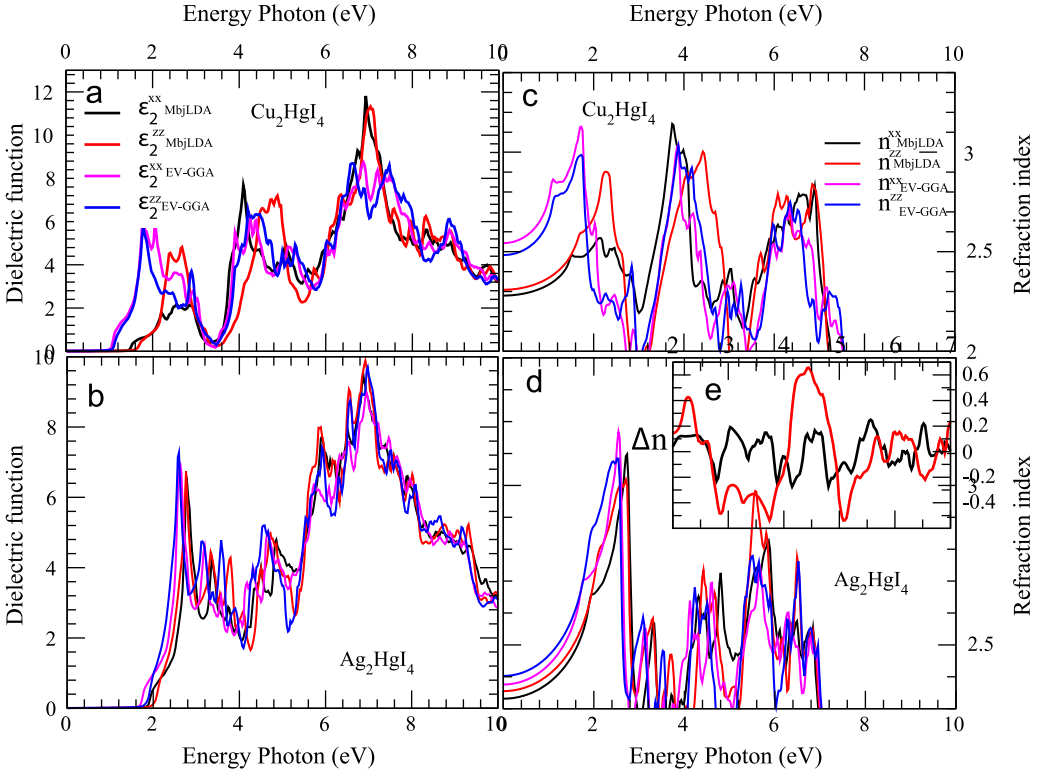

Fig. 8. (a) and (b) Calculated imaginary part of the electronic dielectric function ($\varepsilon_2(\omega)$). (c) and (d) plots represent refractive index for both polarizations $E \perp c$ and $E \| c$. The plot named (e) represents the birefringence dispersion (Δn), line in red for β-$Cu_2Hg\square I_4$ compound and line in black for the β-$Ag_2Hg\square I_4$ one. (For interpretation of the references to color in this figure caption, the reader is referred to the web version of this article.)

Table 1
The lattice constant, a and c, the bulk modulus $B0$ and internal atomic positions $\{u,v,x,y,z\}$ for $Cu_2Hg\square I_4$ and $Ag_2Hg\square I_4$ in its β and defect rock salt structure, along experimental exiting data.

	a (Å)	c (Å)	u	v	x	y	z	$B0$ (GPa)
$Ag_2Hg\square I_4$								
I $\overline{4}$ (LDA)	6.20	12.35	–	–	0.274	0.232	0.137	25.0576
I $\overline{4}$ (GGA)	6.54	13.17	–	–	0.259	0.242	0.130	16.49
I $\overline{4}$ at T=298 K [5]	6.3194	12.606	–	–	0.271	0.229	0.135	–
Defect rocksalt (LDA)	6.14	12.06	–	–	–	–	–	56.4616
Defect rocksalt (GGA)	6.47	12.22	–	–	–	–	–	33.0292
$Cu_2Hg\square I_4$								
I $\overline{4}$ 2 m(LDA)	5.81	11.56	0.285	0.127	–	–	–	29.8514
I $\overline{4}$ 2 m (GGA)	6.13	12.82	0.267	0.134	–	–	–	16.8791
I $\overline{4}$ 2 m at T=298 K [5]	6.0672	12.2266	0.2678	0.1240	–	–	–	–
Defect rocksalt (LDA)	5.75	11.26	–	–	–	–	–	57.4497
Defect rocksalt (GGA)	5.99	11.73	–	–	–	–	–	39.1519

Table 2
mBJ/EV-GGA band gap energy and selected optical properties compared with available experimental data. Refraction index n and second harmonic susceptibility $\chi^{(2)}_{123}$ are calculated at λ=1064 nm.

Crystal	E_g	$n(\lambda=1064)$	$\chi^{(2)}_{123}(\lambda=1064)$ (pm/V)
β-$Cu_2Hg\square I_4$			
exprt	1.96 $\pm$0.04 [43]	2.168 [43]	–
mBJ	1.50	2.309	37.9757
EV-GGA	1.42	2.364	37.1871
β-$Ag_2Hg\square I_4$			
exprt	2.1 [5]	–	–
mBJ	1.9	2.356	21.8237
EV-GGA	1.65	2.403	23.0787

first-order susceptibility tensor $\chi^{(1)}$, namely dielectric function $\varepsilon(\omega)=1+\chi^{(1)}$ (see, for example, our early work [48]). From the above mbj-LDA calculations of band structure, we employ the permitted transitions, namely intra- and inter-band contributions to construct the shape of the dielectric susceptibility. The inter-band transitions can further be split into direct and indirect transitions. Here, we neglect the indirect inter-band transitions which involve scattering of phonon and are expressed to give only small contributions to $\varepsilon(\omega)$. To calculate the direct inter-band contributions to the imaginary parts of the dielectric function $\varepsilon_2(\omega)$, one must sum up all possible transitions from the occupied to the unoccupied states taking into account the appropriate selection rules.

In the case of tetragonal β phases, the symmetry group has two independent components of the dielectric function, namely $\varepsilon^{\parallel}(\omega)$ and $\varepsilon^{\perp}(\omega)$. These frequency dielectric functions correspond to the electric field (**E**) parallel and perpendicular to the crystallographic **c**-axis. We can gain further insight on the dielectric function by examining closely Fig. 8 (a) and (b). It is far easier to notice that the anisotropy between absorptive parts $\varepsilon_2^{\parallel}(\omega)$ and $\varepsilon_2^{\perp}(\omega)$ is very pronounced in the case of $Cu_2Hg\square I_4$ than for $Ag_2Hg\square I_4$. The variation in frequency is expressed in terms of energy, ranging from 0 to 10 eV. According to Fig. 8(a) and (b), the spectrum presents three sharp peaks and some wide ones and its onset are red-shifted by about 7 eV; which defines the screened plasma frequency ω_p, corresponding to the zero crossing of dispersive part of $\varepsilon(\omega)$. Note that we do not include spin–orbit coupling. The latter is expected to split the peaks into weaker sub-peaks. The fundamental gap produces a singularity in $\varepsilon_2(\omega)$ at the threshold energy (first critical point). This point is $\Gamma_v-\Gamma_c$ splitting, which gives the threshold for the direct optical transitions between the highest valence and the lowest conduction band. This is known as the fundamental absorption edge. The origin of this edge is attributed to the interband transitions from the occupied Iodine s states to the unoccupied Ag/Cu-p states.

We move now to extend our prediction to present calculated refractive index gathered in Fig. 8(c) and (d). The purpose of analyzing the spectrum of the refractive index is obvious: from this index we can predict whether the entitled compound can be a siege of phase matching processes. According to the literature [49], a non-centrosymmetric compound showing considerable anisotropy in the linear optical properties, which is useful for SHG and optical parametric oscillation (OPO), due to better fulfilling the phase matching conditions is determined by birefringence. Fig. 8(e) shows the birefringence dispersion for these compounds. It is clear that the birefringence is important only in the non-absorbing spectral range, which is below the energy gap. The birefringence is the difference between the extraordinary and ordinary refraction indices. It can be calculated from the linear response functions from which the anisotropy of the index of refraction is determined. In fact, we find that these crystals possess a positive birefringence at zero energy equal to about 0.1 at $\lambda_f=1064$ nm .

The $Ag_2Hg\square I_4$ and $Cu_2Hg\square I_4$ compounds are yellow at room temperature (β-phase) and become orange above 70 °C in (α-phase) [43]. Optical properties of $Ag_2Hg\square I_4$ have been subject to experimental measures in Ref. [8], but unfortunately no quantitative data are reported. Table 2 gives some optical properties results (calculated and measured) of the β phase of the investigated compounds. A glance to Table 2 shows clearly that the predicted and measured data are in agreement (see also Fig. 9). β phase of the compounds examined in this study has a rather wide energy band gap, situated in the visible range (λ=380–750 nm or E_g=1.65–3.26 eV). The absorption coefficient (see Fig. 9(b)) reveals the radiation absorbing mechanism of the medium. It is found that for the entitled compounds in βstructures, a large

absorption spectrum is observed in the visible light region (above 400 nm). It is clear that these compounds (β phase) seem to have very close absorption patterns. The major contribution is in the range of 400–550 nm, which means that their optoelectronic application can be rather classified in the visible domain (laser or photovoltaic applications). Consequently, further attention on the basic experimental and application of these materials should be directed in this sense. These materials are non-transparent in the visible region and absorptive in the ultraviolet region. Parallel $R_{\parallel}(\omega)$ and perpendicular $R_{\perp}(\omega)$ components of frequency dependent reflectivity versus wavelength for the β-$Ag_2Hg\square I_4$ and β-$Cu_2Hg\square I_4$ compounds are shown in Fig. 9(c). Peaks in the figures show that for each structure there is a maximum value of reflectivity. The maximum lies in the frequency range 250–500 (nm) and arises from the inter band transition. These compounds have reflectivity in the visible and ultraviolet (UV) region of light and can be used as Bragg's reflectors.

The second harmonic response involves 2ω resonance in addition to the usual 1ω resonance. Both 1ω and 2ω resonances can be additionally separated into interband $\chi^{(2)}_{inter}(-2\omega;\omega;\omega)$, intraband $\chi^{(2)}_{intra}(-2\omega;\omega;\omega)$ contributions and the modulation on interband terms by intraband terms $\chi^{(2)}_{mod}(-2\omega;\omega;\omega)$ [50–52] given by

$$\chi^{(ijk)}_{inter}(-2\omega;\omega;\omega)=\frac{e^3}{\hbar^2}\sum_{nml}\int\frac{d\vec{k}}{4\pi^3}\frac{\vec{r}^{\,i}_{nm}\{\vec{r}^{\,j}_{ml}\vec{r}^{\,k}_{nl}\}}{(\omega_{ln}-\omega_{ml})}\times\left\{\frac{2f_{nm}}{(\omega_{mn}-2\omega)}+\frac{f_{ml}}{(\omega_{ml}-\omega)}+\frac{f_{lm}}{(\omega_{ln}-\omega)}\right\}. \quad (5)$$

$$\chi^{(ijk)}_{intra}(-2\omega;\omega;\omega)=\frac{e^3}{\hbar^2}\int\frac{d\vec{k}}{4\pi^3}\sum_{nml}\omega_{nm}\vec{r}^{\,i}_{nm}\{\vec{r}^{\,j}_{ml}\vec{r}^{\,k}_{nl}\}\times\left\{\frac{f_{nl}}{\omega^2_{ln}(\omega_{ln}-\omega)}-\frac{f_{lm}}{\omega^2_{ml}(\omega_{ml}-\omega)}\right\}-8i\sum_{nm}\frac{f_{nm}\vec{r}^{\,i}_{nm}\{\vec{\Delta}^{\,j}_{mn}\vec{r}^{\,k}_{nm}\}}{\omega^2_{mn}(\omega_{mn}-2\omega)}+2\sum_{nml}\frac{f_{nm}\vec{r}^{\,i}_{nm}\{\vec{r}^{\,j}_{ml}\vec{r}^{\,k}_{ln}\}(\omega_{ml}-\omega_{ln})}{\omega^2_{mn}(\omega_{mn}-2\omega)}. \quad (6)$$

$$\chi^{(ijk)}_{mod}(-2\omega;\omega;\omega)=\frac{e^3}{\hbar^2}\int\frac{d\vec{k}}{4\pi^3}\sum_{nml}\frac{f_{nm}}{\omega^2_{mn}(\omega_{mn}-\omega)}\times\{\omega_{nl}\vec{r}^{\,i}_{lm}\{\vec{r}^{\,j}_{mn}\vec{r}^{\,k}_{nl}\}-\omega_{lm}\vec{r}^{\,i}_{nl}\{\vec{r}^{\,j}_{lm}\vec{r}^{\,k}_{mn}\}\}-i\sum_{nm}\frac{f_{nm}\vec{r}^{\,i}_{nm}\{\vec{r}^{\,j}_{mn}\vec{\Delta}^{\,k}_{nm}\}}{\omega^2_{mn}(\omega_{mn}-\omega)}. \quad (7)$$

for all $n\neq m\neq l$. Here, n denotes the valence states, m the conduction states and l denotes all states ($l\neq m,n$). There are two transitions which take place one of them vcc', involving one valence band (v) and two conduction bands (c and c'), which is dominant and the second transition $vv'c$, involving two valence bands (v and v') and one conduction band (c), this transition is weak, so we take only the vcc' transition. The symbols are defined as $\Delta^i_{nm}(\vec{k})=\vartheta^i_{nn}(\vec{k})-\vartheta^i_{mm}(\vec{k})$ with ϑ^i_{nm} being the i component of the electron velocity given as

$$\vartheta^i_{nm}(\vec{k})=i\omega_{nm}(\vec{k})r^i_{nm}(\vec{k}) \quad \text{and}$$

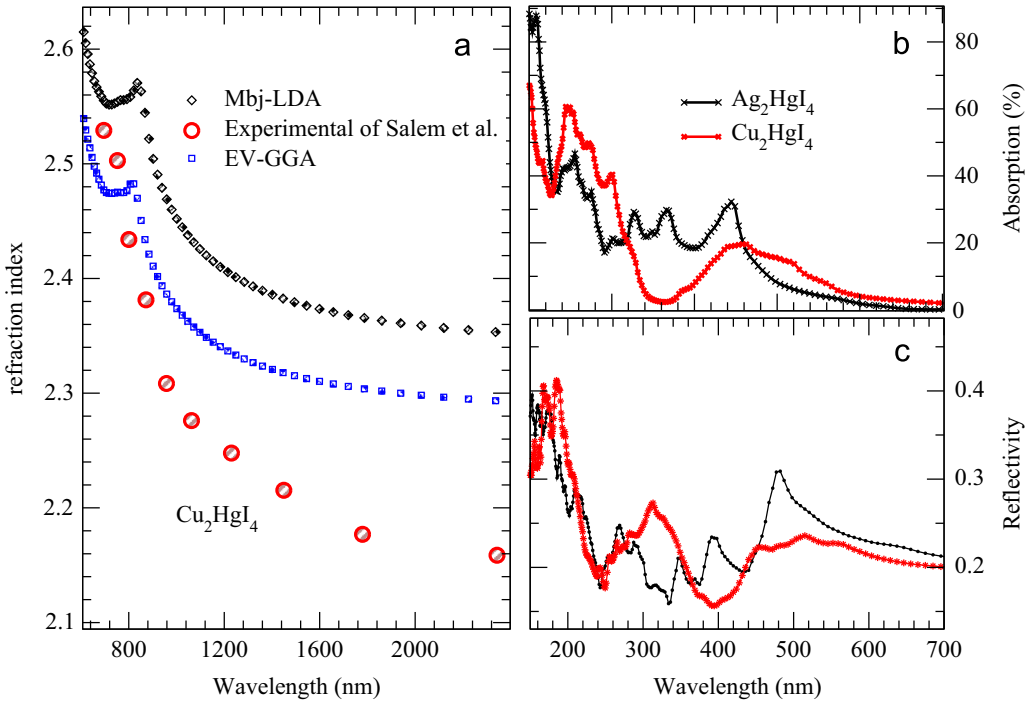

Fig. 9. Calculated of (a) refractive index of β-$Cu_2Hg\square I_4$ compound compared with the experience of Ref. [43] (b) and (c) are receptively absorption and reflectivity as a function of wavelength (nm) of β-$Cu_2Hg\square I_4$ and β-$Ag_2Hg\square I_4$ compounds.

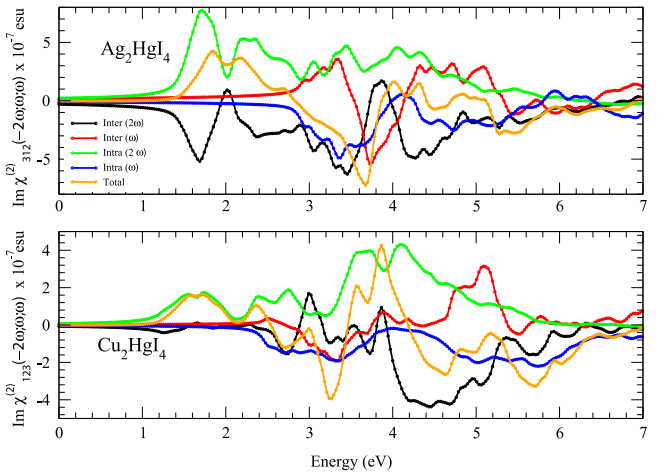

Fig. 10. Calculated total and imaginary part of $\chi^{(2)}_{312}(-2\omega;\omega;\omega)$ and $\chi^{(2)}_{123}(-2\omega;\omega;\omega)$ spectrum along with the intra $(2\omega)/(\omega)$- and inter $(2\omega)/(\omega)$-band contributions for semiconducting phase of the predicted compounds. All $(\mathrm{Im})\chi^{(2)}$ are multiplied by 10^{-7}, in ESU units.

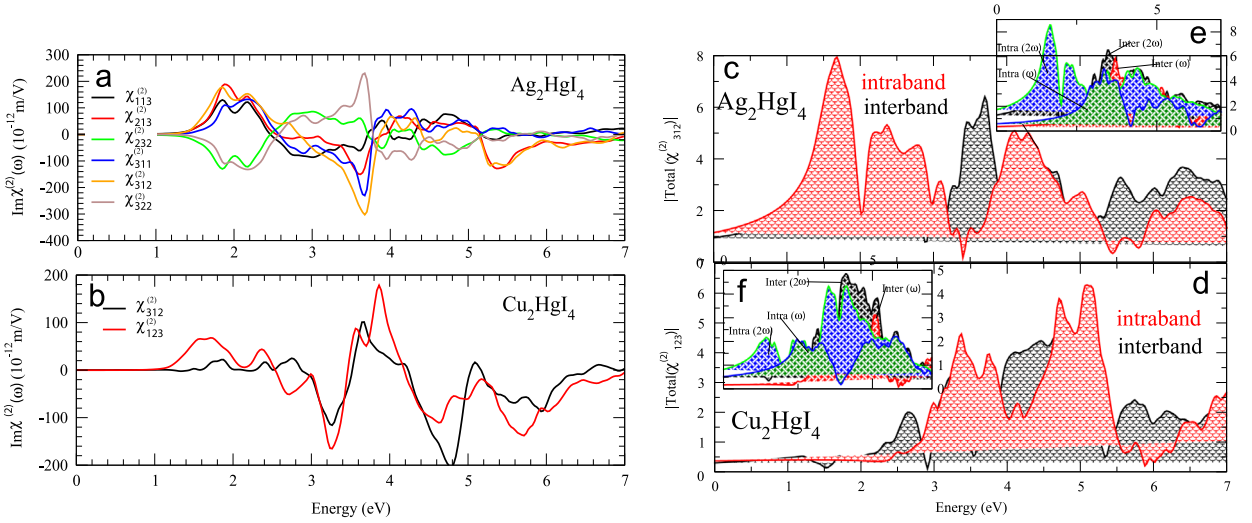

Fig. 11. SHG spectra of the total imaginary of $\chi^{(2)}_{ijk}(-2\omega;\omega;\omega)$ (a) for the β-$Ag_2Hg\square I_4$ and (b) β-$Cu_2Hg\square I_4$ compounds. (c) and (d) plots represent total absolute values of $|\chi^{(2)}_{ikj}|$. (e) and (f) are the absolute values of intra $(2\omega)/(\omega)$- and inter $(2\omega)/(\omega)$-band resonances for both compounds.

$$\{r^i_{nm}(\vec{k})r^j_{ml}(\vec{k})\} = \frac{1}{2}(r^i_{nm}(\vec{k})r^j_{ml}(\vec{k}) + r^j_{nm}(\vec{k})r^i_{ml}(\vec{k})).$$

The position matrix elements between states n and m, $r^i_{nm}(\vec{k})$ are calculated from the momentum matrix element P^i_{nm} using the relation [53]:

$$r^i_{nm}(\vec{k}) = P^i_{nm}(\vec{k})/im\omega_{nm}(\vec{k}). \quad (8)$$

With the energy difference between the states n and m given by $\hbar\omega_{nm} = \hbar(\omega_n - \omega_m)$. $f_{nm} = f_n - f_m$ is the difference of the Fermi distribution functions. Subscripts or superscripts i, j and k are cartesian indices. The real and imaginary parts of the products of matrix elements that control the strength of a given resonance in $\chi^{(2)}_{ijk}(-2\omega;\omega;\omega)$ can be positive or negative [54], see Fig. 10.

Both $Cu_2Hg\square I_4$ stannite and $Ag_2Hg\square I_4$ defect chalcopyrite compounds are structurally derived from a parent structure with 8 symmetric operations. However, their point groups are different. The non-zero coefficients $\chi^{(2)}_{ijk}(-2\omega;\omega;\omega)$ for the $Cu_2Hg\square I_4$ compound with symmetry class (D_{2d}) are $\chi^{(2)}_{123}$ and $\chi^{(2)}_{312}$ (with the following contraction convention: $i\to1$, $j\to2$ and $k\to3$, i, j, and k represent the Cartesian indices). For the $Ag_2Hg\square I_4$ compound with symmetry class (S_4), the independent non-zero components of the SHG under Kleinman assumption are $\chi^{(2)}_{113}$, $\chi^{(2)}_{213}$, $\chi^{(2)}_{232}$, $\chi^{(2)}_{312}$, $\chi^{(2)}_{311}$ and $\chi^{(2)}_{322}$. We established from Fig. 11(a) and (b) that $\chi^{(2)}_{123}$ and $\chi^{(2)}_{312}$ are respectively the dominant components for the $Cu_2Hg\square I_4$ and $Ag_2Hg\square I_4$ compounds.

In Fig. 11(c) and (d), we report the calculated absolute value of $\chi^{(2)}_{312}$ and $\chi^{(2)}_{123}$ for $Ag_2Hg\square I_4$ and $Cu_2Hg\square I_4$,

respectively. Assignment of the peak is done by comparison with the imaginary part of the independent particle dielectric constant ε_2 (Fig. 8(a) and (b)) and interband and intraband contributions gathered in Fig. 11(e) and (f). The SHG presents peaks in energy values of 1.5 and 3.5 eV for the defect chalcopyrite compound, and in energy values of 3.5 and 5 eV for the stannite one. A broad structure between 2.5 and 5.5 eV for both compounds are corresponding respectively to two-photon (2ω) and one-photon (ω) resonances with $\pi \rightarrow \pi^*$ (inter-band) transitions. These peaks between 1 and 3 eV as well as energy around value of 4 eV originate from two-photon (2ω) resonance contributions with $\sigma \rightarrow \sigma^*$ transitions (inter-band). The last structure is mainly associated with the tail in $\varepsilon_2(\omega)$. $\chi^{(2)}_{312}$ and $\chi^{(2)}_{123}$ for $\lambda_f = 1064$ nm are routinely computed and found equal to 37.9757 and 21.8237 (pm/V) for $Cu_2Hg\square I_4$ and $Ag_2Hg\square I_4$, respectively. Unfortunately, no measurements are available for the second harmonic susceptibility for the investigated compounds. Thus, some of predicted results are given for the first time and might be a subject of debate for experimental investigation.

4. Conclusion

Besides the specific characterization of the bonding properties of each of the compounds studied here, there are several interesting features emerging from the overall analysis of the predicted results in this work. One of the most important is the response to an application of pressure. In this paper, we have, successfully, used the Electron localization function analysis to predict the chemical bonding across a phase transition.In addition to the temperature-dependent order–disorder transition reported in the literature at increased pressure, the $Ag_2Hg\square I_4$ and $Cu_2Hg\square I_4$ crystals undergo an order–disorder transformation to a more compact defect rock salt structure; giving rise to a behavior which is experimentally seen in similar compounds, like ($CdGa_2Se_4$, $HgGa_2Se_4$, and $HgGa_2S_4$). This disordered transition induces a decrease of the band gap energy. When moving from β to defect rock salt phase, the compounds show a trend towards non-shared interactions and a softening of the curvatures of the electron density in the bonding regions. Valence electrons become more labile or metallic. In this process, charge transfer decreases and spin localization (ELF) increases reaching the value of $\eta = 0.5$. The location of the attractors is often different from those found in covalent crystals. The reducible valence localization domains form an infinite network over the whole crystal. The channels built in this way can be considered as the region of the space within which the electronic conduction takes place.

Another interesting point addressed in this work was the study of the electro-optic properties. In fact, the calculation using DFT full potential linearized augmented plane wave method within LDA, GGA, EVGGA and mBJ has proved that the semiconducting phase of the $Ag_2Hg\square I_4$ and $Cu_2Hg\square I_4$ compounds possess some interesting features. In fact, the density of states are governed by strong hybridizations between Ag/Cu-*p* and I-*d* states. The calculation of band structure has revealed that both β structures are direct band gap. Our theoretical results of the band gap agree reasonably with the available experimental data. From the band structure prediction we have aimed to present linear and no-linear optical response on the compounds. A rather important part of our arguments has been devoted to clarify the role of interband and intraband contributions in the calculated linear and nonlinear susceptibilities. According to our results, the anisotropy is strong between calculated parallel and perpendicular refractive index. As side finding, the analysis of the optical quantities performed in this work confirms the importance of the second harmonic generation capabilities in the β phase of the $Ag_2Hg\square I_4$ and $Cu_2Hg\square I_4$ compounds. Much work remains to be done on both theoretical and computational fronts. It would be highly desirable to conduct dynamical stabilities under pressure (phonon dispersion or elastic constant calculation) based on the results presented in this work. However, due to the low symmetry and the number of atoms (14 nonequivalent atoms) this task could be numerically very expensive

Acknowledgments

This work is supported by the Algerian Research Program (Cnepru). For A.H. Reshak the result was developed within the CENTEM project, reg. no. CZ.1.05/2.1.00/03.0088, co-funded by the ERDF as part of the Ministry of Education, Youth and Sports OP RDI program. Computational resources were provided by MetaCentrum (LM2010005) and CERIT-SC (CZ.1.05/3.2.00/08.0144) infrastructures.

References

[1] J. Bai, J.M. Raulot, Y.D. Zhang, C. Esling, X. Zhao, L. Zuo, J. Appl. Phys. 109 (2011) 014908.
[2] A.N. Georgobiani, S.I. Radautsan, I.M. Tiginyanu, Sov. Phys. Semicond. 19 (1985) 121.
[3] S.I. Radautsan, I.M. Tiginyanu, Jpn. J. Appl. Phys. 32 (Suppl. 3) (1993) 5.
[4] K.P. Monroe, Ind. Eng. Chcm. 11 (1918) 1116.
[5] S. Hull, Rep. Prog. Phys. 67 (2004) 1233–1314.
[6] J.I. Mcomber, D.F. Shriver, M.A. Ratner, J.R. Ferraro, P. Labonville Walling, J. Phys. Chem. Solids 43 (1982) 903–909.
[7] J.S. Kasper, K.W. Browall, J. Solid. State. Chem. 13 (1975) 49–56.
[8] H.G. LeDuc, L.B. Coleman, Phys. Rev. B 31 (1985) 15.
[9] R. Vilaplana, M. Robledillo, O. Gomis, J.A. Sans, F.J. Manjón, E. Pérez-González, P. Rodríguez-Hernández, A. Muñoz, I.M. Tiginyanu, V.V. Ursaki, J. Appl. Phys. 113 (2013) 073510.
[10] O. Gomis, R. Vilaplana, F.J. Manjón, E. Pérez-González, J. López-Solano, P. Rodríguez-Hernández, A. Munõz, D. Errandonea, J. Ruiz-Fuertes, A. Segura, D. Santamaría-Pérez, I.M. Tiginyanu, V.V. Ursaki, J. Appl. Phys. 111 (2012) 013518.
[11] O. Gomis, R. Vilaplana, F.J. Manjón, D. Santamaría-Pérez, D. Errandonea, E. Pérez-González, J. López-Solano, P. Rodríguez-Hernández, A. Munõz, I.M. Tiginyanu, V.V. Ursaki, J. Appl. Phys. 113 (2013) 073510.
[12] O. Gomis, D. Santamaría-Pérez, R. Vilaplana, R. Luna, J.A. Sans, F.J. Manjón, D. Errandonea, E. Pérez-González, P. Rodríguez-Hernández, A. Muñoz, I.M. Tiginyanu, V.V. Ursaki, J. Alloy Compd. 583 (2014) 70–78.
[13] P.G. Schunemann, T.M. Pollak, J. Cryst. Growth 174 (1997) 278.
[14] K.J. Range, W. Becker, A. Weiss, Z. Naturforsch. B 23 (1968) 1009.
[15] I.I. Burlakov, Y. Raptis, V.V. Ursaki, E. Anastassakis, Solid State Commun. 101 (1997) 377.
[16] V.V. Ursaki, I.I. Burkalov, I.M. Tiginyanu, Y.S. Raptis, E. Anastassakis, A. Aneda, Phys. Rev. B 59 (1999) 257.
[17] S. Meenakshi, V. Vijyakumar, B.K. Godwal, A. Eifler, I. Orgzall, S. Tkachev, H.D. Hochheimer, J. Phys. Chem. Solids 67 (2006) 1660.
[18] S. Meenakshi, V. Vijyakumar, A. Eifler, H.D. Hochheimer, J. Phys. Chem. Solids 71 (2010) 832.
[19] T.F. Fässler, Chem. Soc. Rev. 32 (2003) 80–86.
[20] A. Savin, R. Nesper, S. Wengert, T. Fässler, Angew. Chem. Int. Ed. Engl. 36 (1997) 1809–1832.

[21] B. Silvi, C. Gatti, J. Phys. Chem. A 104 (2000) 947–953.
[22] J. Contreras-García, A. Martín Pendás, B. Silvi, J.M. Recio, J. Theor. Chem. Comp. 113 (2009) 1068.
[23] M. Flórez, M. Marqués, J. Contreras-García, J.M. Recio, Phys. Rev. B 79 (2009) 104101.
[24] A.D. Becke, K.E. Edgecombe, J. Chem. Phys. 92 (1990) 5397.
[25] B. Silvi, A. Savin, Nature 371 (1994) 683.
[26] S. Sharma, J.K. Dewhurst, C. Ambrosch-Draxl, Phys. Rev. B 67 (2003) 165332.
[27] P. Blaha, K. Schwarz, G.K.H. Madsen, D. Kvasnicka, J. Luitz, 2001 wien2k, An Augmented Plane Wave Plus Local Orbitals Program for Calculating Crystal Properties, Vienna University of Technology, Vienna. ISBN 3-9501031-1-2.
[28] J.P. Perdew, A. Zunger, Phys. Rev. 23 (1981) 5048.
[29] J.P. Perdew, K. Burke, M. Ernzerhof, Phys. Rev. Lett. 77 (1996) 3865.
[30] F. Tran, P. Blaha, Phys. Rev. Lett. 102 (2009) 226401–226404.
[31] D. Koller, F. Tran, P. Blaha, Phys. Rev. B 83 (2011) 195134–195143.
[32] P. Dufek, P. Blaha, K. Schwarz, Phys. Rev. B 50 (1994) 7279–7283.
[33] D.J. Singh, Phys. Rev. B. 81 (2010) 195217–195226.
[34] A. Otero-de-la-Roza, E.R. Johnson, V. Luaña, Comput. Phys. Commun. 185 (2014) 1007–1018.
[35] A. MacKinnon, in: O. Madelung, M. Schulz, H. Weiss, (Eds.), Tables of Numerical Data and Functional Relationships in Science and Technology (Landolt-Börnstein New Series, Group III), vol. 17, (Berlin: Springer) p. 124, 1985.
[36] K. Sato, Mater. Sci. Semicond. Process. 6 (2003) 335–338.
[37] A. Otero-de-la Roza, D. Abbasi-Pérez, V. Luaña, Comput. Phys. Commun. 182 (2011) 2232–2248.
[38] F. Tran, P. Blaha, Phys. Rev. Lett. 102 (2009) 226401.
[39] A.D. Becke, E.R. Johnson, J. Chem. Phys. 124 (2006) 221101–221104.
[40] K. Held, O.K. Andersen, M. Feldbacher, A. Yamasaki, Y.-F. Yang, J. Phys.: Condens. Matter 20 (2008) 064202.
[41] L. Hedin, Phys. Rev. 139 (1965) A796.
[42] E. Engel, S.H. Vosko, Phys. Phys. Rev. B 47 (1993) 13164.
[43] A.M. Salem, Y.A. El-Gendy, G.B. Sakr, W.Z. Soliman, J. Phys. D: Appl. Phys. 41 (2008) 025311.
[44] J. Contreras-García, A. Martín Pendás, B. Silvi, J.M. Recio, J. Phys. Chem. Solids 69 (2008) 2204–2207.
[45] R.F.W. Bader, Atoms in Molecules: A Quantum Theory, Oxford University Press, Oxford, 1990.
[46] P. Mori-Sánchez, A. Martín Pendás, V. Luaña, J. Am. Chem. Soc. 124 (2002) 14721–14723.
[47] B. Silvi, C. Gatti, J. Phys. Chem. A 104 (2000) 947–953.
[48] N. Seddiki, T. Ouahran, B. Lasri, T. Benouaz, A.H. Reshak, B. Bouhafs, Mater. Sci. Semicond. Process. 16 (2013) 1454–1465.
[49] I. Merad-Boudia, A.H. Reshak, T. Ouahrani, J. Appl. Phys. 113 (2013) 083505.
[50] J.L.P. Hughes, J.E. Sipe, Phys. Rev. B 53 (1996) 10751.
[51] S.N. Rashkeev, W.R.L. Lambrecht, B. Segall, Phys. Rev. B 57 (1998) 9705–9715.
[52] S. Sharma, J.K. Dewhurst, C. Ambrosch-Draxl, Phys. Rev. B 67 (2003) 165332.
[53] C. Ambrosch-Draxl, J.O. Sofo, Arxiv.: cond-mat/0402523.
[54] M.I. Ziane, Z. Bensaad, T. Ouahrani, B. Labdelli, H.B. Nacer, H. Abid, Mater. Sci. Semicond. Process. 16 (2013) 1138–1147.